Construction and Building Materials 399 (2023) 132488

Contents lists available at ScienceDirect

Construction and Building Materials

journal homepage: www.elsevier.com/locate/conbuildmat

Evaluation of the shear size effect in glued laminated timber using a stochastic FE model calibrated on 17000 glue-line tests

Yuri De Santis [a], Angelo Aloisio [a,*], Dag Pasquale Pasca [b], Massimo Fragiacomo [a], Fabian Dombrowski [b]

[a] Department of Civil, Construction-Architectural and Environmental Engineering, Università degli Studi dell'Aquila, L'Aquila, 67100, Italy
[b] Norsk Treteknisk Institutt (Norwegian Institute of Wood Technology), Børrestuveien 3, 0373 Oslo, Norway

ARTICLE INFO

Keywords:
Glue-line tests
Glued laminated timber
Defect
Size effect
Random field model

ABSTRACT

Glue-line tests provide the shear resistance and failure mode of samples extracted from laminated timber products. Several papers questioned the practical use of such tests affirming the lack of correlation between the capacity of the beam and the outcomes of glue-line tests. However, no studies provide a probabilistic framework for interpreting glue-line tests. This paper presents and discusses the largest database of glue-line tests ever published, consisting of approximately 17000 tests on glued laminated timber (GLT) beams, carried out at the Treteknisk, the Norwegian Institute of Wood Technology (Norway). This database has been used to develop in Abaqus a stochastic FE model to predict the shear capacity of glued laminated timber beams (GLT) using advanced modelling concepts, including discrete cracking and plasticity. The authors examine the dependence of the shear capacity on the beam size to assess the shear size effect in GLT components. The methodology is based on Montecarlo simulations. The mechanical properties of the elementary volumes composing the beam are assigned using a random field model calibrated on the glue-line tests.

1. Introduction

Glued-laminated timber (GLT) is an engineered wood product manufactured by glueing together lumber laminates with a waterproof adhesive. Several approaches have been developed to evaluate the production quality of glued laminated timber (GLT) beams [1–3], such as the delamination tests according to EN 391 [4] and shear tests on core samples according to EN 392, [5]. In addition, recent research also considered the prospect of employing ultrasound-based techniques to detect defects in GLT [6].

Shear tests provide the glue-line strength in existing structures from circular core samples according to EN 392 [5] or ASTM D 905-03 [7]. The information on the core samples is used to extrapolate at a global scale the member strength. The shear test equipment applies a load parallel to the glue-line. The test delivers two key properties: the shear strength obtained by dividing the estimated capacity by the specimen size and the failure mode. The failure mode expresses the percentage of glue, wood or fibre failure from visual inspections. The two pieces of information can be associated with the bonding quality. For example, there are several requirements on the strength of glue-lines depending on the percentage of wood failure [8,9], i.e. a higher rate of glue failure leads to higher requirements on the strength.

There has yet to be a consensus on the optimal size and shape of the core specimen and the extraction method. Selbo [10] found that cylindrical specimens extracted perpendicular to the glue-lines exhibited a 14% lower shear strength than standard block specimens, according to ASTM D 905-03 [7]. Outinen and Koponen [11] developed a method for samples extracted perpendicular to the glue-lines, proving that the shear strength values of drilled specimens were significantly higher (30%–70%) than block specimens. Gaspar et al. [12] also showed a size effect for the average shear strength of block specimens. Feuerer [13] questioned the reliability of a vision-based approach for the percentage of wood failure evaluation on more than 1000 core samples taken from 81 engineering timber structures and on newly produced glued-laminated timber. Feuerer [13] proposed a correction factor based on beam height.

Most importantly, several studies affirm that there is no correlation between the shear capacity of a beam and the extracted glue-line core samples. Specifically, Scharmacher [14] carried out shear tests on 31 GLT beams according to EN 408 [5], 31 delamination tests according to EN 391 [15], and 93 shear tests according to EN 392 [5] on samples taken from the beams. He deduced that, despite the tests on core samples providing helpful information to evaluate the glue-lines, they

* Corresponding author.
E-mail addresses: yuri.desantis@univaq.it (Y. De Santis), angelo.aloisio1@univaq.it (A. Aloisio), dpa@treteknisk.no (D.P. Pasca), massimo.fragiacomo@univaq.it (M. Fragiacomo), fabian.dombrowski@treteknisk.no (F. Dombrowski).

https://doi.org/10.1016/j.conbuildmat.2023.132488
Received 29 April 2023; Received in revised form 7 July 2023; Accepted 10 July 2023
Available online 24 July 2023

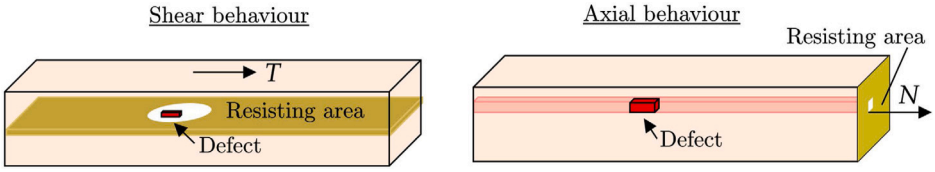

Fig. 1. Illustration of the size effects under axial and shear forces.

could not be used to predict the shear strength due to the lack of a significant correlation. This result was confirmed by Tannert et al. [16], showing the lack of correlation between the strength of GLT beams and the shear strength of the glue-lines. Tannert et al. [16] severely criticize the practice of deriving the strength of glued laminated timber beams based on the glue-line strength of core samples tested according to EN 392 and evaluated according to EN 396. In contrast, Schulte-Wrede et al. [17] found a good correlation between the shear capacity of full-scale beams and core samples after assuming an exponent of 0.2 for taking into account the size effect [18]. Nonetheless, the number of tests in [17] is very limited and cannot be used to infer the size effect reliably.

Large members tend to fail at lower stresses than smaller members loaded similarly [19]. The effect of size on wood properties [20–23] is often referred to as size-effect and also known from other building materials, e.g. concrete [24–26]. Different causes lead to a size effect. One is related to the natural variability of timber due to the random distribution of growth characteristics, such as distinct knots or knot clusters denoted as defects. Materials with a distinct heterogeneity, such as concrete, can also exhibit a deterministic size effect related to the scale of the inherent material heterogeneity [27–29].

Size effects in GLT are mainly related to defect distribution. Most studies on GLT focus on the bending size effect. In bending, the weakest link theory can be applied to estimate the dependence of the bending strength on the element size [30,31]. Foschi and Barrett [32] applied the weakest link theory to the shear strength of lumber and developed a design formula incorporated into CSA-086 (Canadian Standards Association 1980, 1984). Nonetheless, while there is a consensus on the size effect in bending, the size effect in shear is more challenging to understand. Accordingly, the Eurocode only considers the bending size effect adopting the k_h parameter, neglecting the shear-related one. The k_h factor originates from Weibull's strength theory [33], referring to strength as a statistical property and expressing the probability of brittle failure based on weak points within a stressed volume. Additionally, most recent numerical [34–36] and experimental [37–42] studies focus on bending size effect, based on complex stochastic strength models.

Compared to other engineering fields, in timber engineering, there is an unbalance between the research towards understanding the size effect in bending vs shear [28]. The main reason behind this knowledge gap is the prevalent size effects in bending, as illustrated in Fig. 7. In timber, the size effect is related to the probability of a defect occurrence and the loading scenario [34,43]. Under axial forces, a flaw impairs the strength of the entire wood fibre [44]. Conversely, a fibre imperfection under shear forces only partially compromises the stress distribution along the shear plane (see Fig. 1). Therefore, the size effect is more evident when the axial forces are more prominent than the shear forces.

However, this does not mean it does not exist since no study systematically investigated uncertainty propagation from the spatial strength distribution to the shear capacity in the context of nonlinear fracture mechanics [45–49].

Years from 2009 to 2015 saw a significant advancement in the stochastic FE models representative of the complex variability of GLT properties [50–55]; see the finite element (FE)-based stochastic GLT strength model [23,56] implemented in the Julia programming language [57] Tapia [56]. For instance, Vida et al. [36] included the lamination effect [58], accounting for the reinforcing of weak points by neighbouring lamellas, the local failure mechanisms between the lamellas based on the micromechanical model proposed by Hofstetter et al. [59], and the geometric reconstruction algorithm proposed by Kandler et al. [60]. Such models mainly simulated typical loading scenarios involving mixed shear-bending failure. To the author's knowledge, no research developed advanced FE models based on nonlinear fracture mechanics [61,62] to isolate the size effect in shear.

There are two main reasons supporting the practical importance of understanding the shear size effect in GLT:

- The dimensions of GLT beams are continuously increasing to realize wide-span hall constructions or flexible office buildings. However, experimental investigations of large beams are unavailable because of the tremendous effort involved. Therefore, a database of tests on large beams loaded in shear must be developed.
- The design considers independent bending and shear verification. Therefore, isolating the size effects in the two loading scenarios is essential. Unfortunately, this has yet to be done so far for shear. Typical experimental tests lead to a mixed shear-bending failure. Thus, it is impossible to ascertain the size effects of shear forces.
- The scientific literature presents contradictory results. Tannert et al. [16] found a lack of correlation, while others observed a prominent dependence [63]. These incongruities cannot be accepted and depend on limits on both sides. The influence of defects on the shear size effect is far more complex than bending. It demands a statistical framework for interpreting the uncertainty propagation of glue-line tests to the shear capacity of a beam.

The path towards a comprehensive understanding of the shear-related size effect in GLT still needs time and effort. In the lack of experimental tests on big-sized beams, numerical simulation campaigns represent a necessary alternative to understanding the shear size effect. A phenomenon dominated by uncertainty cannot be understood as deterministic. To the authors' knowledge, no probabilistic model calibrated on an extensive database of glue-line tests was used to develop a stochastic GLT model for assessing shear phenomena in GLT beams in the framework of nonlinear fracture mechanics. This paper attempts to narrow the mentioned gaps by providing the following original contributions.

- Presentation and discussion of the largest database on glue-line tests ever published, nearly 17 000 tests, consisting of dry samples extracted from GLT elements.
- Development of a probabilistic interpretative framework of the tests based on bimodal Weibull distributions. Such a model considers the failure mode dependence on the shear strength. Such an extensive database is fundamental to properly calibrate the extreme values of the probability density functions, which trigger the cracks. The glue-line tests give information on the spatial variability of the shear strength of beam segments.
- Development of a random field model to generate a nonlinear fracture mechanics stochastic FE model, where the shear strength distribution in the shear plane is discretized into 25 mm × 25 mm cells. This model provides a first assessment of the shear-related size effect in GLT, to be further validated by experimental shear tests on GLT beams. In addition, the preliminary results give an insight into the spatial propagation of the shear strength uncertainty on the beam shear capacity.

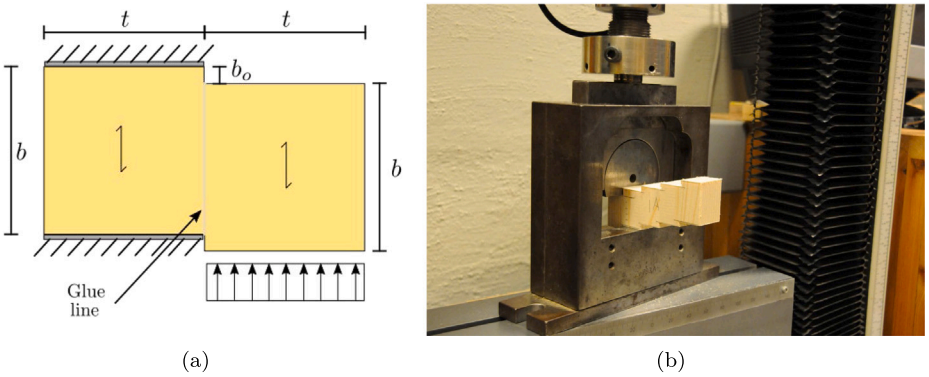

Fig. 2. (a) Description of the experimental test and (b) View of an ongoing test.

Fig. 3. View of a typical timber (a) and glue (b) failures.

Table 1
Shear strenght requirement according to JAS.

Failure	Shear strength	Wood failure ratio
Class 3 (Douglas fir)	7.2 N/mm^2	65%
Class 5 (Spruce & Pine)	6.0 N/mm^2	65%

2. Description of the dataset

The Norwegian Institute of Wood Technology (Norway) conducts "block shear tests" according to the Japanese Agricultural Standard, MAFF notification no. 683, on samples having a glue area of 25 mm × 25 mm, see Fig. 2(a). The samples are obtained from a GLT element by sawing a stepped sample, shown in Fig. 2(b). The testing machine applies a vertical load corresponding to each step so that the sliding plane corresponds to the step angle. According to the Japanese standard, the minimum requirements are reported in Table 1.

The primary outcomes of the tests are (i) the peak resistance, (ii) the shear strength obtained by dividing the maximum force by the specimen size, and (iii) the percentage of failures. They indicate the percentage of wood, glue or fibre failure. The rates of failure are generally estimated visually with the aid of a microscope. Fig. 3 shows a typical timber (a) and glue failure (b). It is important to note that the figure was not acquired using a microscope.

Fibre failure is rare and corresponds to the tensile rupture of the fibres alongside their mutual sliding. This failure condition cannot be readily estimated and requires a microscope. The very active role of Treteknisk in Japanese certifications provides the authors with an unusually vast database of glue-line tests on various GLT strength classes, with the following types of glues: PRF adhesives (Phenol Resorcinol Formaldehyde), EPI adhesives (Emulsion Polymerized Isocyanate), MF adhesives (Melamine Formaldehyde), MUF adhesives (Melamine Urea Formaldehyde), PUR adhesives (Polyurethane reactive adhesive), RF (Resorcinol Formaldehyde).

The adhesive composition in the considered database predominantly consists of 50% MUF (Melamine Urea Formaldehyde) and MF (Melamine Formaldehyde), 35% EPI (Emulsion Polymerized Isocyanate) and 15% PRF (Phenol Resorcinol Formaldehyde) adhesives. PRF adhesives are renowned for their exceptional durability and water resistance, making them ideal for high-strength and weather-resistance applications. On the other hand, MUF adhesives provide robust bonding strength and resistance to moisture. They find extensive use in manufacturing engineered wood products, such as plywood, particleboard, and medium-density fiberboard (MDF). To comply with the standard requirements, the samples within the database are conditioned to attain a moisture content ranging from 8% to 15% before conducting the testing. While no specific statistics regarding the moisture distribution of the specimens are available, the samples underwent the necessary moisture conditioning to adhere to the established standards.

In this paper, the authors will not analyze the differences between the different types of glues, which exhibited similar performances [46, 64].

The total number of tests considered in this study is 16 997, resulting from certification activities from 2018 to 2022. Table 2 groups the data by the observed failure mechanism associated with the wood glue or fibre failure. Specifically, the authors identified a failure type only if the percentage exceeds 0.8. Otherwise, it has been classified as mixed. It must be remarked that the dataset also comprises data with shear strength lower than 4 MPa, which is generally associated with a defect. The considerable amount of data has an exceptional value for

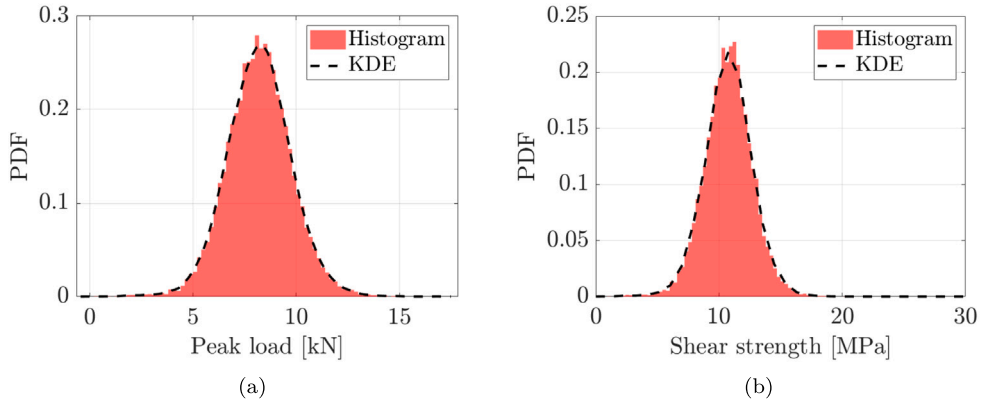

Fig. 4. Histogram plots of (a) the peak load and (b) the shear strength for the considered database.

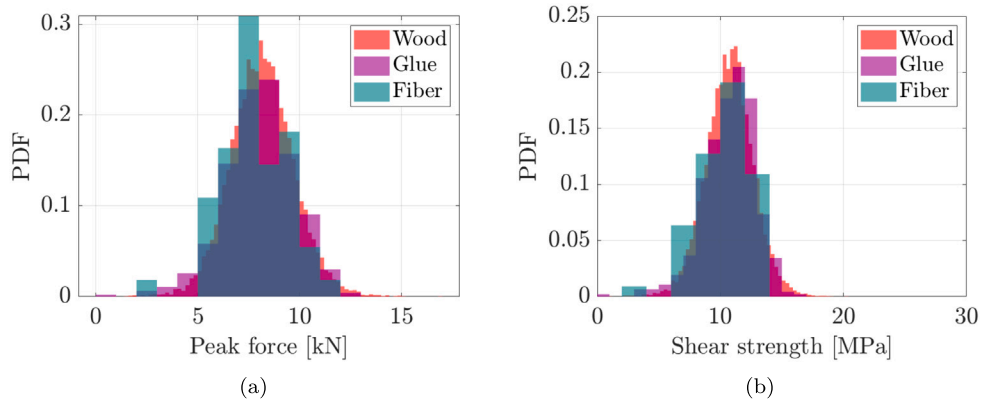

Fig. 5. Histogram plots of (a) the peak load and (b) the shear strength for the considered database distinguished by the types of failures.

Table 2
Data classification based on the observed failure mechanism.

Failure	Percentage	No of samples
Wood	97.37%	16 550
Glue	2.21%	376
Fibre	0.03%	5
Mixed (<0.8)	0.39%	66
Total		16 997

accurately characterizing the low-side extreme values responsible for the defects trigger.

The classification in Table 2 proves the following:

- The percentage of wood failure is dominant and approximately 97%, followed by the glue with an approximate 2% rate of loss. The fibre failure can be considered negligible. Therefore, the two failure mechanisms to be reasonably considered in a predictive model are the wood and glue strength.
- The mixed failure types are sporadic. The failure is generally of one type. Therefore, the failure mechanism can be reasonably considered independent of each other.

Fig. 4 shows the histogram plots of the peak load (a) and the shear strength (b) for the considered database. As anticipated, the considerable size of the database also allows us to characterize the tails of the distributions. The histograms have been fitted almost perfectly with the kernel density.

The same data can be visualized by distinguishing between the failure mode, wood, glue or fibre (see Fig. 5). The histogram plots are somewhat overlapped. Likely, the failure mode does not depend on the shear strength. Nonetheless, this appears valid only when the shear strength exceeds 4–5 MPa. In that situation, the percentages of wood and glue failure are nearly 97 and 2%, respectively. When the strength value is lower than 4 MPa, the rate of glue failure significantly increases, almost reaching 100% for strength values lower than 1 Mpa. This result is clearly shown in Fig. 6. While the bar plot in Fig. 6(a) accurately represents the percentages of failure at higher strengths, Fig. 6(b) plots the failure rate for wood and glue as a function of the strength.

The fibre failure is always very low and generally independent of the strength. Conversely, the wood and glue failure rates are markedly dependent on the strength. Lower strength values are associated with a defect, which impairs the glue strength more than the wood strength. This evidence could be related to the bridging effect of the fibres close to the defect, absent if the flaw manifests in the glue-line.

The simulation of the failure rate dependence on the strength value can be obtained with Weibull distributions for the wood and glue strength. Nonetheless, as highlighted in the following paragraphs, such a peculiar trend is difficult to obtain with two Weibull distributions. Furthermore, using two Weibull distributions, the inversion point in the failure rate is too close to the histogram peaks. Therefore, bimodal Weibull distributions are necessary to accurately seize the inversion point of the failure rates at approximately 2 Mpa and the kernel density of the shear strength. The following section presents the mathematical formulation developed for interpreting the considered database.

3. Problem formulation

The mathematical problem is formulated in two steps. First, the authors show the probabilistic model adopted to describe the glue-line shear strength. The second shows that the shear strength can be viewed

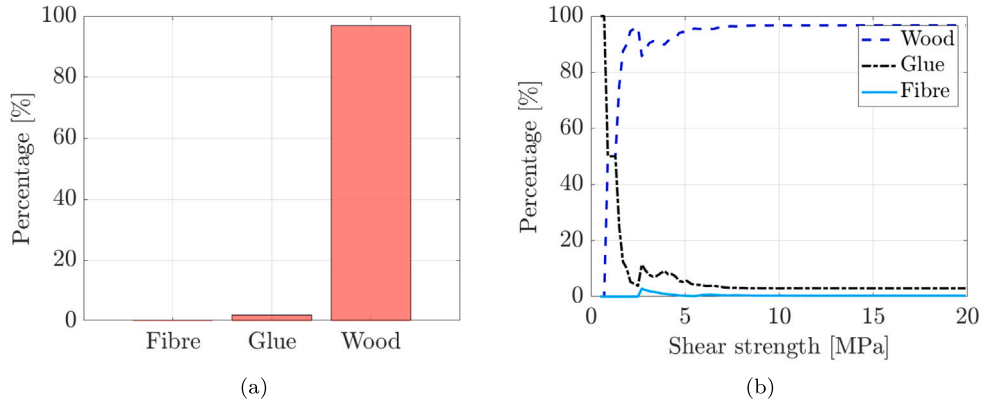

Fig. 6. (a) Bar plot of the percentage of failure from all samples and (b) variation of them as a function of the shear strength in MPa.

as a random function defined over the spatial domain of a generic GLT element.

3.1. Probabilistic model for the glue-line shear strength

The generic random variable representative of the shear resistance of ith element can be written as:

$$X_i = \min(X_{T,i}, X_{G,i}, X_{F,i}) \tag{1}$$

where $X_{T,i}, X_{G,i}, X_{F,i}$ are three continuous and positive random variables expressing the shear resistance in case of timber, glue or fibre failure. The experimental results show that a few cases exhibit a mixed failure mode, while the three failure modes are treated as independent random variables. Additionally, the fibre failure is negligible and has been neglected in the analysis.

The generic random variable expressing the shear resistance in case of wood failure can be described as a bimodal probability distribution:

$$X_{T,i} \propto P_T \left[\frac{\kappa_{T,r}}{\lambda_{T,r}} \left(\frac{X_{T,i}}{\lambda_{T,r}} \right)^{\kappa_{T,r}-1} e^{-(X_{T,i}/\lambda_{T,r})^{\kappa_{T,r}}} \right] + (1 - P_T) \left[\frac{\kappa_T}{\lambda_T} \left(\frac{X_T}{\lambda_T} \right)^{\kappa_T - 1} e^{-(X_{T,i}/\lambda_T)^{\kappa_T}} \right] \tag{2}$$

P_T expresses the probability that the random variable $X_{T,i}$ follows the Weibull density function $\left[f\left(p, \lambda_{T,r}, \kappa_{T,r}\right) \right]$, and $\lambda_{T,r}, \kappa_{T,r}$ are the size and shape parameters of a Weibull probability distribution describing the low-values strength. Parallelly, $1 - P_T$ expresses the probability that the random variable $X_{T,i}$ follows the probability density function f, with parameters λ_T, κ_T. P_T physically expresses the probability that a defect occurs in the timber-side failure. Analogously the shear resistance in case of glue failure can be written as:

$$X_{G,i} \propto P_G \left[\frac{\kappa_{G,r}}{\lambda_{G,r}} \left(\frac{X_{G,i}}{\lambda_{G,r}} \right)^{\kappa_{G,r}-1} e^{-(X_{G,i}/\lambda_{G,r})^{\kappa_{G,r}}} \right] + (1 - P_G) \left[\frac{\kappa_G}{\lambda_G} \left(\frac{X_G}{\lambda_G} \right)^{\kappa_G - 1} e^{-(X_{G,i}/\lambda_G)^{\kappa_G}} \right] \tag{3}$$

To avoid the solution of an ill-posed inverse problem, it is assumed that the following holds:

$$P_T = P_G = P_F = P_D \tag{4}$$

The unknown parameters of the probability distributions describing the two random variables can be collected in the following vector

$$\boldsymbol{p} = \left\{ P_D, \lambda_T, \kappa_T, \lambda_{T,r}, \kappa_{T,r}, \lambda_G, \kappa_G, \lambda_{G,r}, \kappa_{G,r} \right\} \tag{5}$$

The unknown parameters can be determined by minimizing the following objective function:

$$\boldsymbol{p} = \underset{\boldsymbol{p}}{\operatorname{argmin}} \left(OF_p + OF_T + OF_G \right) \tag{6}$$

where the three terms of the objective function are:

$$OF_p = \mathrm{KDE}_{exp} - \mathrm{KDE}_{sim} \tag{7}$$

where KDE_{exp} and KDE_{sim} are the Kernel density functions describing the empirical distributions of the experimental and simulated values of the random variable X_i. OF_T and OF_G express the rate of failures as a function of the stress, as displayed in Fig. 6(b):

$$OF_T = P_{exp,T}(\tau_f) - P_{sim,T}(\tau_f) \tag{8}$$

where $P_{exp,T}(\tau_f)$, and $P_{sim,T}(\tau_f)$ are empirical probability functions describing the probability of a wood-type failure mode as a function of the shear strength (τ_f) for the experimental and simulated data, respectively.

$$OF_G = P_{exp,G}(\tau_f) - P_{sim,G}(\tau_f) \tag{9}$$

where $P_{exp,G}(\tau_f)$, and $P_{sim,G}(\tau_f)$ are empirical probability functions describing the probability of a glue-type failure mode as a function of the shear strength (τ_f) for the experimental and simulated data, respectively.

The optimization problem in Eq. (6) has been solved using a classical metaheuristic optimization algorithm, the genetic algorithm implemented in Matlab [65].

The proposed model predicts the shear strength and the failure mode, wood or glue-line.

3.2. Random field model

To model the spatial distribution of the shear strength with a random field, the GLT member is discretized into N surface elements dS, with an area corresponding to that of the specimens cut for glue-line tests. Accordingly, the random field is discretized into a set of correlated random variables that represent the value of the random field over each surface element. Among the several methods available in the literature for the discretization of random fields, the midpoint method is used in the analysis because of its numerical stability and straightforward implementation [66].

Specifically, for the discretization, a timber element with length L and width W is assumed to be a single independent area [67] divided into $N = X \times Y$ surface elements with size 25×25 mm^2, where X and Y are the number of elements in the x and y directions, (see Fig. 7). The coordinates of its centroid identify the ith surface element dS_i in the Cartesian plane spanning the length and width of the structural component, respectively, i.e, $dS_i = dS(x_i, y_i)$. Fig. 7 displays a representation of the adopted discretization.

According to the proposed discretization, the value of the shear strength f_i in each surface element is given by a stationary random field with constant mean μ and covariance $\Sigma(\mathbf{x}, \sigma^2, \boldsymbol{\theta})$, where $\mathbf{x}$ contains the

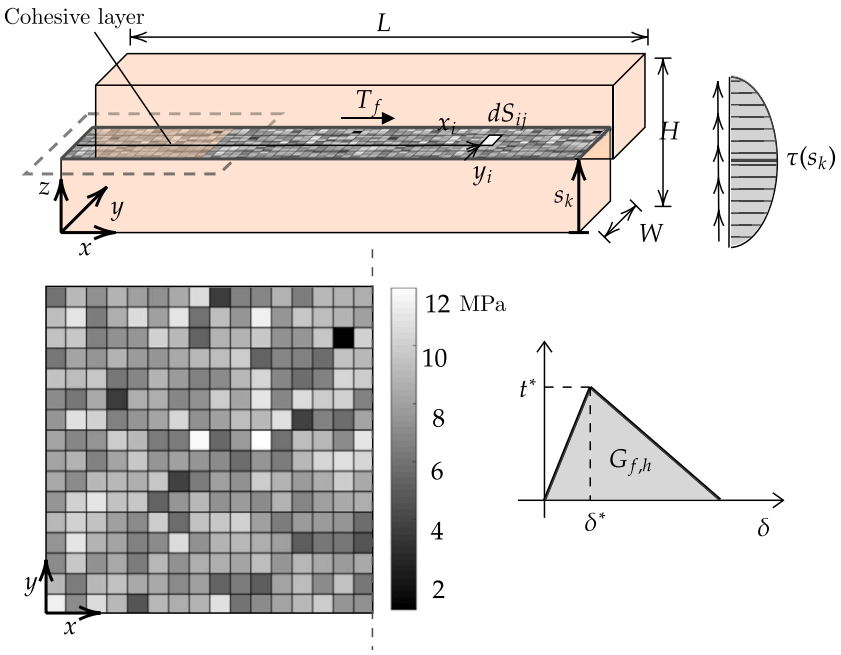

Fig. 7. Schematic illustration of the discretized shear strength model for GLT.

centroids of all the surface elements. Specifically, the generic element of the covariance is defined as

$$\left[\boldsymbol{\Sigma}\left(\mathbf{x},\sigma^2,\boldsymbol{\theta}\right)\right]_{ij}=\sigma^2 C_{ij}\left(\mathbf{x},\boldsymbol{\theta}\right), \tag{10}$$

where σ^2 is the variance previously derived, which is assumed constant, neglecting any degradation effect on the material, and the type B correlation function

$$C_{ij}\left(\mathbf{x}_{ij},\boldsymbol{\theta}\right)=\exp\left[-\left(\frac{x_i-x_j}{\theta_x}\right)^2-\left(\frac{y_i-y_j}{\theta_y}\right)^2\right] \tag{11}$$

is chosen to assume a separable correlation structure and corresponds to a spatial extension of the Gaussian correlation function [68] widely used for defining material properties [69]. In Eq. (11), $\mathbf{x}_{ij}$ contains the centroids of the ith and jth surface elements and $\boldsymbol{\theta}=(\theta_x,\theta_y)$ are the correlation lengths in the x and y directions, respectively. Since no data is available on the correlation lengths, their values are derived from "engineering judgment".

3.3. Finite element model

The mechanical behaviour of a GLT beam loaded in shear is reproduced by means of a three-dimensional finite element model (Fig. 7). The authors fixed all degrees of freedom of the beam on the lower side, ensuring complete constraint. Similarly, except for horizontal translation, all degrees of freedom are also fully constrained on the upper side of the beam. Additionally, a uniformly distributed horizontal force has been applied on the upper side of the beam, parallel to the lamination plane. It is worth noting that this static scheme enables the isolation of the pure effect of shear while disregarding those associated with bending.

The timber lamellas are discretized through linear brick elements with reduced integration, namely C3D8R of ABAQUS/Standard library. A cubic mesh of a size of 5 mm was found to be the most adequate by sensitivity studies, a good trade-off between accuracy and computational effort. Timber constitutive law is linear elastic with properties defined according to EN-338 [70]. The elasticity and shear moduli corresponding to the timber class GL28 h of the tested specimens are used and reported in Table 3.

Shear longitudinal cracks between lamellas are simulated using a cohesive contact within the Extended Finite Element Method (XFEM) framework. The XFEM-based cohesive method can be used to simulate crack initiation and propagation along an arbitrary path with almost no mesh dependence [71,72] and it is suitable for the simulation of both glue and timber failure [73]. The cohesive surface defined in the longitudinal plane is discretized in squared cells with a dimension of 25 mm × 25 mm. For each cell, cohesive contact allows reproduction of the elastic behaviour that verifies until damage initiation and damage evolution until complete failure. The elastic behaviour is described using a stiffness tensor whose components are defined in Table 4 as a function of timber elastic properties. The damage initiation criterion is defined by the following equation:

$$\frac{\tau}{f_l}=1 \tag{12}$$

where τ is the shear stress and f_l is the cell shear failure stress defined according to the sampling methodology. The damage evolution is defined by a linear law and the fracture energy $G_{f,h}$. The fracture energy value reported in Table 4 descends from literature [36]. Viscous regularization has been used to overcome convergence difficulties caused by the softening behaviour. Using viscous regularization, the tangent stiffness matrix of the cohesive contact is positive for sufficiently small time increments. The relaxation time of the viscous system is represented by the viscosity parameter η_h whose value is reported in Table 4.

All adjacent lamellas of the beam can theoretically experience horizontal cracking. The authors simulate the shear response of a beam by applying two opposing shear forces on the two free boundaries, as displayed in Fig. 7. This loading scenario induces a shear failure along an unknown sliding plane. Accordingly, only horizontal cracks arise in the developed model to eliminate bending-related phenomena.

Table 3
Timber mean elastic properties: longitudinal and perpendicular Young's modulus and longitudinal and rolling shear modulus.

Lamellas		
E_l	N/mm^2	12 600
E_p	N/mm^2	300
G_l	N/mm^2	650
G_p	N/mm^2	65

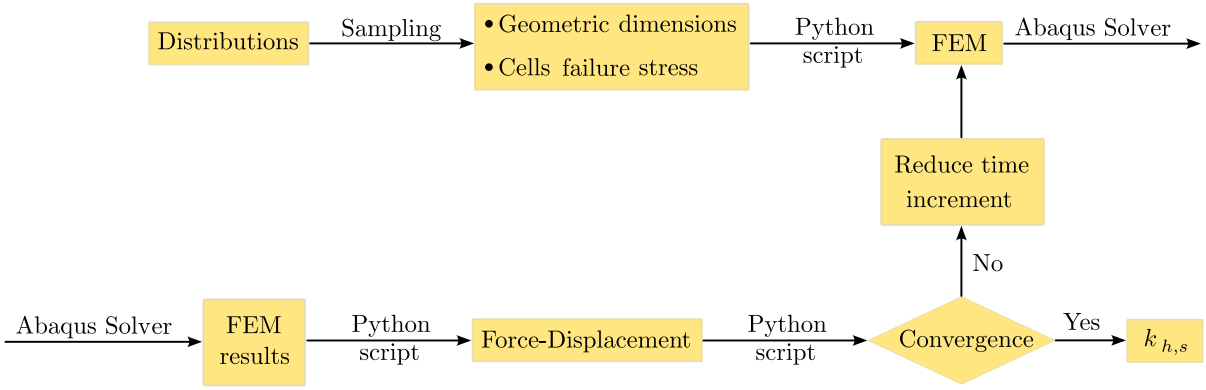

Fig. 8. Flowchart of stochastic FE simulations.

Table 4
Stiffness tensor components k_l and k_p, shear strength f_{ij} , fracture energy $G_{f,h}$, and viscosity coefficient η_h.

k_l	N/mm^3	650
k_p	N/mm^3	65
$f_l = f_{ij}$	N/mm^2	Randomly sampled from a Normal distribution
$G_{f,h}$	N/mm^2	0.6
η_h		10^{-9}

To perform Montecarlo simulations, the procedure described in the flowchart of Fig. 8 was implemented. Each model is generated using Python according to the required geometrical and mechanical inputs. A geometrically linear static incremental analysis is performed. At the end of the analysis, the results in terms of force displacement are extracted, and convergence is assessed by checking for the existence of a softening branch. If the analysis does not converge, the maximum step increments are iteratively reduced to reach convergence. When convergence is reached, the analysis results regarding failure loads are saved.

The shear-related size factor ($k_{h,s}$) can be estimated as follows:

$$k_{h,s} = \frac{T_f(\boldsymbol{x}, \boldsymbol{\theta})}{T_{f,ref}(\boldsymbol{x})} \tag{13}$$

where $T_f(\boldsymbol{x}, \boldsymbol{\theta})$ is the shear capacity obtained from the stochastic GLT shear strength model, and $T_{f,ref}(\boldsymbol{x})$ is the reference shear capacity obtained by assuming a constant shear strength for all cells equal to the expected value of the probabilistic model. $\boldsymbol{x}, \boldsymbol{\theta}$ identify the deterministic and random parameters. In this situation, the random variable is the shear strength, defined by a Gaussian stationary random field. The methodology followed in this paper can be summarized as follows:

- Calibration of the parameters of the bimodal probability density functions using a genetic optimization algorithm;
- Montecarlo simulation of the random field model to predict the shear capacity of the GLT beam as a function of its size.
- Estimation of the shear size effect as a function of the GLT size.

4. Results

This section is partitioned into two subsections. The first is on the calibration of the probabilistic model, and the second is on the outcomes of the stochastic FE simulations.

4.1. Probabilistic model calibration

The proposed probabilistic model in Eq. (1) predicts the shear strength and the failure mode of the GLT specimen. The number of parameters to be calibrated is the size and scale parameters of the four Weibull distributions and the probability value P_F corresponding to the bimodal definition in Eqs. (2), (3). All the parameters collected in Eq. (5) are estimated using a genetic optimization algorithm. Fig. 9 plots the results of the optimized model. The optimized model with parameters in Table 5 is overlapped with the experimental estimations of the percentages of failure (a) and shears strength (b).

Table 5
Optimal parameters of the bimodal probabilistic model developed to interpret the glue-line tests, where LU and UB are the lower and upper bounds, respectively.

Parameter	Initial value	LB	UP	Optimum
P_D	0.01	0.1	0.00001	0.001
λ_T	10	20	0.1	9.67
κ_T	5	20	0.1	5.77
$\lambda_{T,r}$	1	20	0.1	1.06
$\kappa_{T,r}$	0.4	20	0.1	8.34
λ_G	19	20	0.1	17.61
κ_G	5	20	0.1	6.45
$\lambda_{G,r}$	1	20	0.1	13.42
$\kappa_{G,r}$	0.8	20	0.1	0.45

The main reason for choosing a bimodal rather than a classical Weibull distribution originates from the variation of the percentage of failure as a function of the shear strength. The inversion point, i.e., where the wood and glue failure rate equals 50%, is approximately 1 MPa. It is practically impossible to obtain an inversion point at 1 Mpa using a classical Weibull distribution for the glue and wood shear resistance. The inversion point is too far from the distribution peak and is associated with shallow probability values. Using two mono-modal Weibull functions for the wood and glue shear strength, the inversion point would be close to 5 MPa. If the scholars forced the optimization to follow only the relative percentages of failure, the peak would be shifted and close to 4 Mpa. Therefore, the authors adopted this solution to accurately reproduce the failure percentage types at a low strength value.

This model can be used to predict with reasonable accuracy the failure modes as a function of the shear strength. However, the glue and wood failure percentages are constant in the ranges of interest higher than 4 MPa, where most samples are gathered. Therefore, it would be a useless complication to develop a random field model using the proposed model since only the shear strength of each cell is required in the stochastic FE model. Therefore, the authors also provided the parameters of a fitting Gaussian distribution, optimized from genetic optimization: mean (μ) 8.2 MPa, and standard deviation (σ) equal to 1.48 MPa.

As shown in Fig. 10, the distribution accurately fits the normalized histogram of the experimental data. However, it cannot provide the dependence of the failure mode on the shear strength. The authors propose both models since they could have different applications. The first is for interpreting experimental data on GLT samples, and the second is for random field modelling.

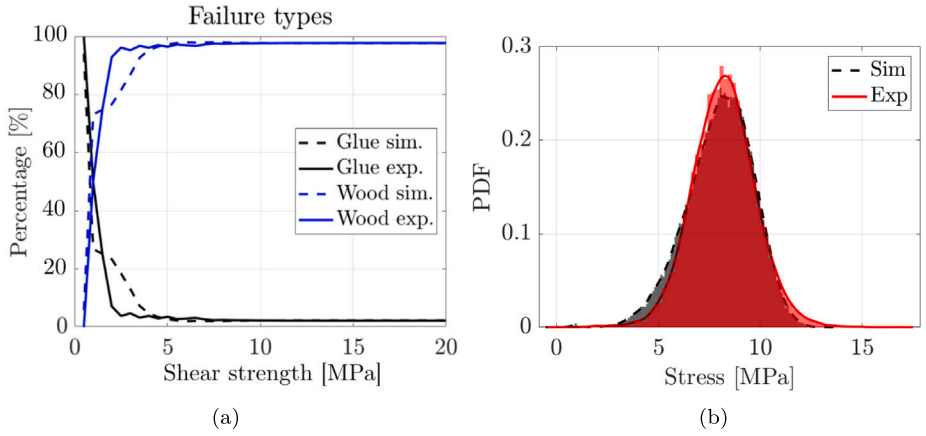

Fig. 9. (a) Variation of the glue and wood failure percentages as a function of the shear strength; (b) Superposition between the experimental and simulated values of the shear strength using the probabilistic model in Eq. (1) with parameters in Table 5.

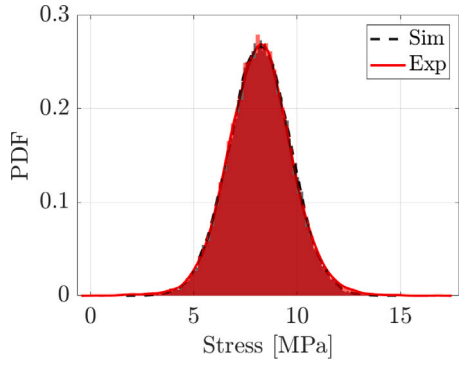

Fig. 10. Prediction of the experimental data distribution using a Normal PDF with a mean (μ) 8.2 and standard deviation (σ) equal to 1.48.

Table 6
Input parameters of the Monte Carlo simulations, where L and U denote the lower and upper bounds of the uniform distributions, t and l are the thickness and length of the shear plane, respectively.

Symbol	Distribution	Characteristics	
t [mm]	Uniform	L = 100	U = 400
l [mm]	Uniform	L = 1000	U = 5000
f_{ij} [MPa]	Eq. (11)		

4.2. Montecarlo analyses using FE model

The authors estimated the GLT beam shear capacity, assuming the shear strength uncertainty from the random field model of the shear strength and the beam size. The GLT size at each step is simulated by randomly sampling the length, width and height from the uniform probability distributions in Table 6.

The shear size effect is estimated by simulating a block shear test where the size of the shear plane is randomly sampled from uniform probability density functions representing the length and thickness of the beam. Three Montecarlo analyses are carried out, following Table 7. In the first set, the shear strength of each cell is sampled from a Gaussian density function mean (μ) 8.2 MPa, and standard deviation (σ) equal to 1.48 MPa, ignoring the effect of spatial correlation. The second and the third analyses consider the effect of spatial correlation assuming two sets of correlation length, reported in Table 7. Since no scientific paper deals with estimating the random field parameters to simulate the shear capacity, the authors assume two limit situations characterized by a high and low spatial correlation, respectively. Additionally, it is assumed that the spatial correlation is higher in the direction parallel to the grain and lower in the orthogonal direction to imitate the timber anisotropy. Specifically, the first simulation assumed θ_x = 600 mm and θ_y = 60 mm, while the second θ_x = 10 mm and θ_y = 1 mm. Fig. 11 shows two representations of the random field generated assuming the two sets of parameters, characterizing a high and low spatial correlation, respectively.

Table 7
List of analyses and related parameters of the random field.

No	θ_x [mm]	θ_y [mm]	σ [MPa]
1	No random field		
2	600	60	1.48
3	10	1	1.48

A higher spatial correlation leads to a lower probability of a defect occurrence and vice-versa. The FE simulations are carried out in Abaqus, where the mechanical and geometric parameters are parametrized. In addition, the authors exploit the interoperability between Abaqus and Python to import random generations of the geometry and the corresponding values of the shear strength for each cell. The typical stress-slip response is shown in Fig. 12a together with contour-plots of the shear stresses evolution on the sliding plane for increasing slip (Fig. 12b). The crack initiation point can be easily identified in Fig. 12b. After the crack initiation, the load suddenly reduces due to crack propagation. It is worth noting that the crack tends to propagate to the nearest cells before other cracks can form in other areas of the plane. A stress concentration area can be observed around the formed crack. This behaviour was observed in all simulations. In none of the cases, a segmented force–displacement curve was observed that could have indicated the contemporary formation of multiple failure points. This behaviour indicates that the stress re-distribution along the sliding may be negligible and a shear size effect might exist.

The primary outcome of the analysis is the shear strength, obtained by dividing the shear capacity and the area of the sliding plane, following Eq. (14). The shear strength is then plotted against the area of the shear plane to ascertain the shear size effect. An exponential function in Eq. (14) is then used to fit the results and estimate the size effect coefficient.

$$\tau_f = \frac{T_f}{A_s} \rightarrow \quad \hat{\tau}_f = a \cdot \exp(-b \cdot A_s) + 6 \tag{14}$$

Fig. 13 plots the results of the three sets of Montecarlo analyses, as shown in Table 7.

The primary outcomes of the investigation can be itemized in the following bullet points.

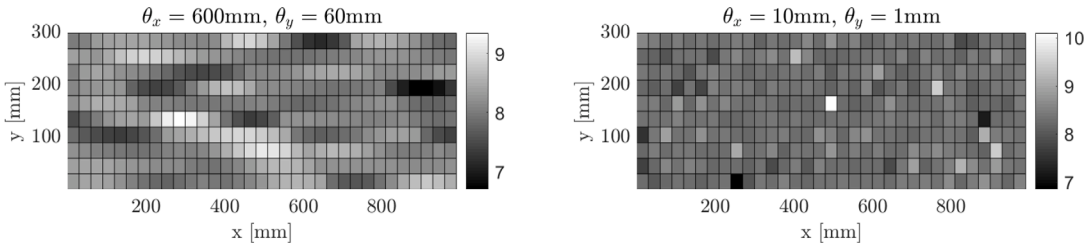

Fig. 11. Random field representation of the shear strength with different choices of the correlation lengths. The values are in MPa.

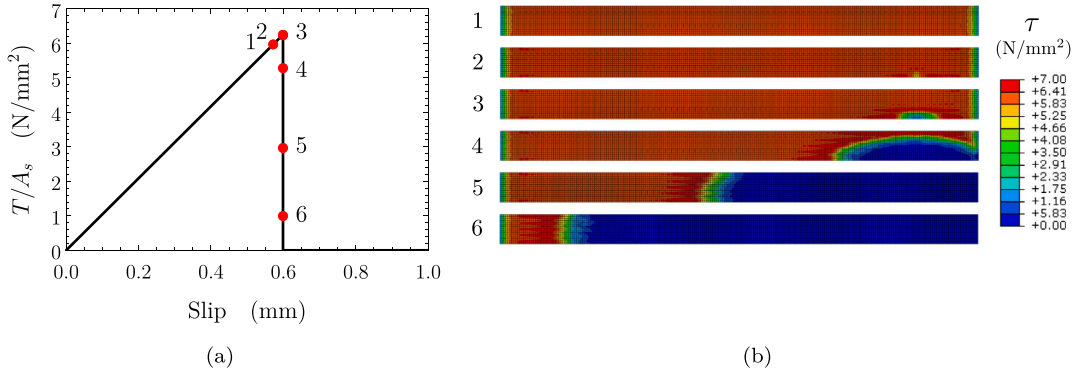

Fig. 12. Typical finite element model simulation: (a) average stress vs slip and (b) stresses on fracture plane for increasing slip.

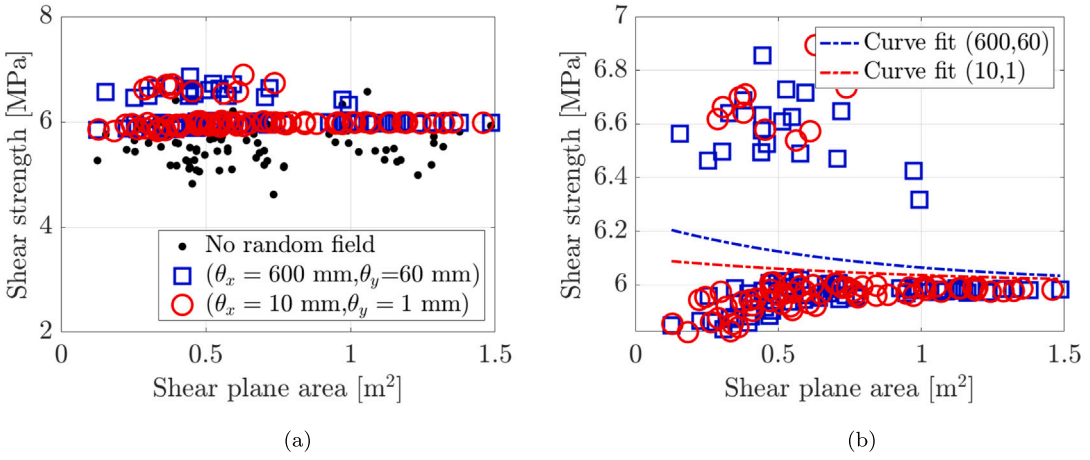

Fig. 13. (a) Shear strength as a function of the area of the sliding plane, according to the configurations in Table 7 and (b) corresponding curve fitting.

- The mean shear strength for all simulations is approximately 6 MPa, while the mean shear strength of each cell is 8.2 MPa, following the adopted Gaussian random field. This means that the shear capacity is not the mere summation of the shear capacity contributions of each cell. Otherwise, the average capacity of the simulated specimen would be 8.2 MPa. The presence of cells with a lower shear strength significantly affects the global shear behaviour of the specimen, leading to an approximate 2 MPa reduction of the shear strength compared to the glue-line tests on 30 mm × 30 mm specimens.
- In the considered ranges of variation of the area of the shear plane, the size effect is quite limited since, also for small-size specimens, the capacity never exceeds 7 MPa. Nonetheless, the size effect is rather evident since small-size samples exhibit, on average, higher shear strength than the larger ones. This effect almost extinguishes if the area of the sliding plane exceeds 1 m^2. Additionally, if the sliding plane is lower than 1 m^2, there are two data clusters. In the absence of a weak cell, the shear strength rises to almost 6.5 MPa, while in the presence of weak cells, the shear strength is lower than 6 MPa. This phenomenon is in line with expectations. The consequences of a defect are higher in small specimens, whether it exists or not. Conversely, if the sliding plane is more extensive than 1 m^2, a fault is very likely to occur, and the shear strength tends to be an asymptote at 6 MPa.
- As expected, there is no size effect in the simulations, not considering the spatial correlation, since a defect is equally probable to occur in the small and big specimens. Conversely, the size effect manifests when a random field model is considered. Nonetheless, the outcomes of the two random field models are similar. As expected, the size effect is more prominent with a higher spatial correlation when $\theta_x = 600$ mm and $\theta_y = 60$ mm.

The author fitted the experimental results using an exponential function in Eq. (14), where the unknown parameters are a and b. The offset parameter is assumed to equal 6, given the evidence that the shear strength tends to be an asymptote at 6 Mpa. Table 8 shows the estimated coefficients of the fitting curves with 95% confidence bounds.

Table 8
Coefficients of Eq. (14) with 95% confidence bounds.

θ_x [mm]	θ_y [mm]	a	b
600	60	0.2415 (−0.05344, 0.5365)	1.327 (−1.036, 3.691)
100	10	0.1006 (−0.133, 0.3342)	1.025 (−3.195, 5.245)

They have been estimated using the Levenberg–Marquardt optimization algorithm.

The fitting functions define a size effect coefficient for shear $k_{h,s}$. For the sake of simplicity, the authors adopted a step-wise definition. If the sliding pane is lower than 1 m^2, the exponential function can be used. Otherwise, it can be considered constant and equal to 0.73. It is essential to recognize that the regression model while providing a useful average representation, cannot fully capture the distinct characteristics of each branch. Thus, it should be acknowledged that the resulting regression curve represents an intermediate behaviour rather than accurately describing either of the two branches.

$$k_{h,s} = \begin{cases} 0.73 \cdot \left[1 + \frac{a}{c} \cdot \exp(-b \cdot A_s)\right] & \text{if } A_s \leq 1 \text{ m}^2 \\ 0.73 \text{ if } A_s > 1 \text{ m}^2 \end{cases} \quad (15)$$

This coefficient expresses the reduction of shear strength from the small specimen, without defects, to the structural element with a higher probability that lower shear strength values arise. In most cases, the shear plane is more extensive than one m^2, although the considered simulations are ideal due to the assumption of the failure mode. In practical cases, the failure originates from mixed shear-bending failure. This investigation aimed to isolate the size shear effect to clarify its role in design. The analyses reveal that the shear strength is significantly reduced compared to the glue-line tests. The asymptotic relationship between shear strength and shear plane area showed in Fig. 13b is confirmed by the experimental studies conducted by Rammers et al. [74,75], by Longworth [76] and by the American plywood association [77]. These studies highlighted that big-sized beams have lower shear strength.

5. Conclusions

The paper presents a comprehensive probabilistic framework for interpreting the largest database of glue-line tests ever collected, comprising 17,000 specimens from Gl28 h Glued Laminated Timber (GLT). The study focuses on understanding the failure modes, whether glue or wood side, and their dependence on shear strength. The analysis reveals that as shear strength exceeds 4 MPa, both glue and wood failure rates stabilize at approximately 2% and 98%, respectively. This finding highlights the strong influence of shear strength on the failure mode distribution in GLT. To develop a practical model, a simplified probabilistic approach based on Gaussian fitting is employed to create a random field model for shear strength. This model is then integrated into a stochastic finite element simulation for further analysis. Additionally, the authors investigate the size effect in the shear capacity of GLT beams by running a Montecarlo analysis. This analysis involves randomly sampling beam sizes and generating a Gaussian shear strength random field. The outcomes of this investigation provide valuable insights into the statistical impact of beam size on shear capacity. The results indicate that, in design considerations, the shear size effect can generally be considered negligible. However, it is observed that the shear strength is approximately 30% lower compared to values obtained from the glue-line tests. This finding is consistent with the shear strength values suggested by both standards and producers, which tend to be lower than the average value of 8.2 MPa obtained from homogeneous GLT of class 28 in the glue-line tests. Overall, the study offers a comprehensive probabilistic framework that advances our understanding of the failure modes and shear capacity in GLT.

CRediT authorship contribution statement

Yuri De Santis: Writing – review & editing, Writing – original draft, Visualization, Validation, Supervision, Software, Resources, Project administration, Methodology, Investigation, Funding acquisition, Formal analysis, Data curation, Conceptualization. **Angelo Aloisio:** Writing – review & editing, Writing – original draft, Visualization, Validation, Supervision, Software, Resources, Project administration, Methodology, Investigation, Funding acquisition, Formal analysis, Data curation, Conceptualization. **Dag Pasquale Pasca:** Writing – review & editing, Writing – original draft, Visualization, Validation, Software, Resources, Project administration, Methodology, Investigation, Funding acquisition, Formal analysis, Data curation, Conceptualization. **Massimo Fragiacomo:** Supervision. **Fabian Dombrowski:** Resources, Project administration, Investigation, Funding acquisition, Data curation.

Declaration of competing interest

All authors have participated in (a) conception and design, or analysis and interpretation of the data; (b) drafting the article or revising it critically for important intellectual content; and (c) approval of the final version.

This manuscript has not been submitted to, nor is under review at, another journal or other publishing venue.

The authors have no affiliation with any organization with a direct or indirect financial interest in the subject matter discussed in the manuscript.

Data availability

Data will be made available on request

References

[1] S. Aicher, G. Dill-Langer, Non-Destructive Detection of Glue Line Defects in Glued Laminated Timber, Vol. 1, 2008, pp. 254–261, cited By 3.
[2] S. Sanabria, C. Mueller, J. Neuenschwander, P. Niemz, U. Sennhauser, Air-coupled ultrasound as an accurate and reproducible method for bonding assessment of glued timber, Wood Sci. Technol. 45 (4) (2011) 645–659, http://dx.doi.org/10.1007/s00226-010-0357-z, cited By 37.
[3] T. Tannert, T. Vallée, S. Hehl, Experimental and numerical investigations on adhesively bonded timber joints, Wood Sci. Technol. 46 (1–3) (2012) 579–590, http://dx.doi.org/10.1007/s00226-011-0423-1, cited By 29.
[4] Glued laminated timber - performance requirements and minimum production requirements, 2001, cited By 61.
[5] Timber structures - structural timber and glued laminated timber - determination of some physical and mechanical properties, 1995, cited By 623.
[6] D. Sandberg, G. Fink, J. Hasener, M. Kairi, T. Marhenke, R.J. Ross, R. Steiger, X. Wang, Process control and grading in primary wood processing, in: Springer Handbook of Wood Science and Technology, Springer, 2023, pp. 1019–1073.
[7] Standard test method for strength properties of adhesive bonds in shear by compression loading, 2003, cited By 168.
[8] Glued laminated timber, in: Performance Requirements and Minimum Production Requirements, 2001, cited By 3.
[9] Standard practice for estimating the percentage of wood failure in adhesive bonded joints, 2003, cited By 1.
[10] M. Selbo, A new method for testing glue joints of laminated timber in service, Forest Prod. J. 12 (2) (1962) 65–67, cited By 3.
[11] K. Outinen, S. Koponen, Drilled shear specimen (DSS), in: Proceedings of Conference on COST E13, 2001, cited By 1.
[12] F. Gaspar, H. Cruz, A. Gomes, Evaluation of Glued Laminated Timber Structures - Core Extraction and Shear Testing, Vol. 3, 2008, pp. 1533–1540, cited By 2.
[13] M. Feuerer, Beurteilung von brettschichtholz im bestand beziehungen von kleinproben und tragwerk, 2009, cited By 1.
[14] F. Scharmacher, Untersuchungsmethoden zur bestimmung der klebstofffugenqualität, 2011, cited By 1.
[15] Glued laminated timber - shear test of glue lines, 1995, cited By 36.
[16] T. Tannert, T. Vallée, A. Müller, Critical review on the assessment of glulam structures using shear core samples, J. Civ. Struct. Health Monit. 2 (2012) 65–72.
[17] M. Schulte-Wrede, M. Merk, P. Dietsch, Experimental investigation on the shear resistance of existing glulam structures, in: 5th International Conference on Structural Health Assessment of Timber Structures SHATIS, 2019.

[18] R. Brandner, W. Gatternig, G. Schickhofer, Determination of shear strength of structural and glued laminated timber, in: Proc. of the CIB-W18 Meeting, Vol. 45, 2012.

[19] B. Madsen, A.H. Buchanan, Size effects in timber explained by a modified weakest link theory, Can. J. Civil Eng. 13 (2) (1986) 218–232.

[20] L. Blank, G. Fink, R. Jockwer, A. Frangi, Quasi-brittle fracture and size effect of glued laminated timber beams, Eur. J. Wood Wood Prod. 75 (5) (2017) 667–681, http://dx.doi.org/10.1007/s00107-017-1156-0, cited By 18.

[21] M. Brunetti, M. Nocetti, B. Pizzo, F. Negro, G. Aminti, P. Burato, C. Cremonini, R. Zanuttini, Comparison of different bonding parameters in the production of beech and combined beech-spruce CLT by standard and optimized tests methods, Constr. Build. Mater. 265 (2020) http://dx.doi.org/10.1016/j.conbuildmat.2020.120168, cited By 10.

[22] C.-H. Wang, Y.-k. Wen, Reliability and redundancy of pre-northridge low-rise steel buildings under seismic excitation, 1998, na.

[23] C. Tapia, S. Aicher, Survival analysis of tensile strength variation and simulated length-size effect along oak boards, J. Eng. Mech. 148 (1) (2022) http://dx.doi.org/10.1061/(ASCE)EM.1943-7889.0002006, cited By 2.

[24] P. Nallathambi, B. Karihaloo, B. Heaton, Various size effects in fracture of concrete, Cem. Concr. Res. 15 (1) (1985) 117–126, http://dx.doi.org/10.1016/0008-8846(85)90016-X, cited By 50.

[25] Y. Zhang, H. Li, A. Abdelhady, J. Yang, H. Wang, Effects of specimen shape and size on the permeability and mechanical properties of porous concrete, Constr. Build. Mater. 266 (2021) http://dx.doi.org/10.1016/j.conbuildmat.2020.121074, cited By 24.

[26] W. Luo, J.-L. Le, M. Rasoolinejad, Z. Bažant, Coefficient of variation of shear strength of rc beams and size effect, J. Eng. Mech. 147 (2) (2021) http://dx.doi.org/10.1061/(ASCE)EM.1943-7889.0001879, cited By 12.

[27] A. Hillerborg, M. Modéer, P.-E. Petersson, Analysis of crack formation and crack growth in concrete by means of fracture mechanics and finite elements, Cem. Concr. Res. 6 (6) (1976) 773–781.

[28] Z.P. Bazant, M.T. Kazemi, et al., Size effect on diagonal shear failure of beams without stirrups, ACI Struct. J. 88 (3) (1991) 268–276.

[29] Z. Bazant, Z. Li, Modulus of rupture: Size effect due to fracture initiation in boundary layer, J. Struct. Eng. (US) 121 (4) (1995) 739–746, http://dx.doi.org/10.1061/(ASCE)0733-9445(1995)121:4(739), cited By 98.

[30] B. Bohannan, Effect of Size on Bending Strength of Wood Members, Vol. 56, Forest Product Lab./USDA Forest Service, 1966.

[31] J. Barrett, Effect of size on tension perpendicular-to-grain strength of douglas-fir, Wood Fiber Sci. (1974) 126–143.

[32] R.O. Foschi, J. Barrett, Longitudinal shear strength of douglas-fir, Can. J. Civil Eng. 3 (2) (1976) 198–208.

[33] W. Weibull, 1939. cited By 1.

[34] G. Fink, A. Frangi, J. Kohler, Probabilistic approach for modelling the load-bearing capacity of glued laminated timber, Eng. Struct. 100 (2015) 751–762.

[35] M. Frese, H. Blaß, Statistics of damages to timber structures in Germany, Eng. Struct. 33 (11) (2011) 2969–2977, http://dx.doi.org/10.1016/j.engstruct.2011.02.030, cited By 30.

[36] C. Vida, M. Lukacevic, G. Hochreiner, J. Füssl, Size effect on bending strength of glued laminated timber predicted by a numerical simulation concept including discrete cracking, Mater. Des. 225 (2023) 111550.

[37] R. Falk, K. Solli, E. Aasheim, The Performance of Glued Laminated Beams Manufactured from Machine Stress Graded Norwegian Spruce, Rep. No. 77, 1992, cited By 13.

[38] E. Aasheim, K. Solli, Size factor of norwegian glued laminated beams, Size Factor Nor. Glued Laminated Beams (1995) cited By 2.

[39] R. Pischl, G. Schickhofer, C. Seiner, A. Steinberger, E. Gehri, R. Mauritz, Entwicklung leistungsfähiger holzleimbauteile: Zusammenfassender bericht zum FFF-forschungsprojekt, FFF-forschungsprojekt, Graz/A – Zürich/CH – Wien/A, 1995, cited By 1.

[40] G. Fink, J. Kohler, A. Frangi, Bending tests on glued laminated timber beams with well-known material properties, 2013, cited By 12.

[41] G. Kandler, M. Lukacevic, J. Füssl, Experimental study on glued laminated timber beams with well-known knot morphology, Eur. J. Wood Wood Prod. 76 (5) (2018) 1435–1452, http://dx.doi.org/10.1007/s00107-018-1328-6, cited By 14.

[42] G. Fink, P. Stadelmann, A. Frangi, Bending test on large-scale GLT beams with well-known beam setup using machine grading indicator, Int. Wood Prod. J. 12 (4) (2021) 258–266, http://dx.doi.org/10.1080/20426445.2021.1969166, cited By 1.

[43] S. Aicher, Fracture and size effect law for spruce and oak in mode I and mixed mode I and II, in: Proceedings of the RILEM TC133 Meeting, LRBB, Bordeaux, France, 1992, cited By 1.

[44] L. Blank, G. Fink, R. Jockwer, A. Frangi, Quasi-brittle fracture and size effect of glued laminated timber beams, Eur. J. Wood Wood Prod. 75 (2017) 667–681.

[45] L. Daudeville, Fracture in spruce: Experiment and numerical analysis by linear and non linear fracture mechanics, Holz Roh Werkstoff 57 (6) (1999) 425–432, http://dx.doi.org/10.1007/s001070050068, cited By 40.

[46] H. Dorn, K. Egner, Brandversuche an brettschichtverleimten holzträgern unter biegebeanspruchung, Eur. J. Wood Wood Prod. 25 (8) (1967) 308–320.

[47] G. Fink, J. Kohler, Probabilistic modelling of the tensile related material properties of timber boards and finger joint connections, Eur. J. Wood Wood Prod. 73 (3) (2015) 335–346, http://dx.doi.org/10.1007/s00107-015-0895-z, cited By 9.

[48] G. Fink, J. Kohler, Model for the prediction of the tensile strength and tensile stiffness of knot clusters within structural timber, Eur. J. Wood Wood Prod. 72 (3) (2014) 331–341, http://dx.doi.org/10.1007/s00107-014-0781-0, cited By 26.

[49] C. Gebhardt, M. Kaliske, Fracture simulation of timber structures using xfem, in: Proceedings of the EUROMECH Colloquium 556 on Theoretical, Numerical, and Experimental Analyses in Wood Mechanics, Dresden, 2015, pp. 16–17, cited By 1.

[50] P. Guindos, M. Guaita, A three-dimensional wood material model to simulate the behavior of wood with any type of knot at the macro-scale, Wood Sci. Technol. 47 (3) (2013) 585–599, http://dx.doi.org/10.1007/s00226-012-0517-4, cited By 64.

[51] C. Jenkel, M. Kaliske, Finite element analysis of timber containing branches - An approach to model the grain course and the influence on the structural behaviour, Eng. Struct. 75 (2014) 237–247, http://dx.doi.org/10.1016/j.engstruct.2014.06.005, cited By 24.

[52] M. Lukacevic, J. Füssl, Numerical simulation tool for wooden boards with a physically based approach to identify structural failure, Eur. J. Wood Wood Prod. 72 (4) (2014) 497–508, http://dx.doi.org/10.1007/s00107-014-0803-y, cited By 62.

[53] M. Lukacevic, J. Füssl, R. Lampert, Failure mechanisms of clear wood identified at wood cell level by an approach based on the extended finite element method, Eng. Fract. Mech. 144 (2015) 158–175, http://dx.doi.org/10.1016/j.engfracmech.2015.06.066, cited By 46.

[54] L. Qiu, E. Zhu, J. Van De Kuilen, Modeling crack propagation in wood by extended finite element method, Eur. J. Wood Wood Prod. 72 (2) (2014) 273–283, http://dx.doi.org/10.1007/s00107-013-0773-5, cited By 36.

[55] J. Schmidt, M. Kaliske, Models for numerical failure analysis of wooden structures, Eng. Struct. 31 (2) (2009) 571–579, http://dx.doi.org/10.1016/j.engstruct.2008.11.001, cited By 96.

[56] C. Tapia, S. Aicher, Survival analysis of tensile strength variation and simulated length–size effect along oak boards, J. Eng. Mech. 148 (1) (2022) 04021130.

[57] J. Bezanson, A. Edelman, S. Karpinski, V.B. Shah, Julia: A fresh approach to numerical computing, SIAM Rev. 59 (1) (2017) 65–98.

[58] N. Nakamura, K. Fujita, Simulation method to generate the strength of glulam using correlated random variables, J. Wood Sci. 57 (2011) 203–207.

[59] K. Hofstetter, C. Hellmich, J. Eberhardsteiner, Micromechanical modeling of solid-type and plate-type deformation patterns within softwood materials. A review and an improved approach, 2007.

[60] G. Kandler, M. Lukacevic, J. Füssl, An algorithm for the geometric reconstruction of knots within timber boards based on fibre angle measurements, Constr. Build. Mater. 124 (2016) 945–960.

[61] S. Aicher, H. Reinhardt, Influence of structure size in linear and nonlinear (wood) fracture mechanics [einflußder bauteilgröße in der linearen und nichtlinearen (holz-)bruchmechanik], Holz Roh Werkstoff 51 (3) (1993) 215–220, http://dx.doi.org/10.1007/BF02628282, cited By 31.

[62] R. Leicester, The size effect of notches, in: Proc. 2 Australasian Conf. on Mech. of Struct. Mater nd, 1969, pp. 41–420, cited By 27.

[63] R. Brandner, P. Dietsch, J. Dröscher, M. Schulte-Wrede, H. Kreuzinger, M. Sieder, G. Schickhofer, S. Winter, Shear properties of cross laminated timber (CLT) under in-plane load: Test configuration and experimental study, in: INTER Proceedings Meeting 48 2015, 2015, pp. 181–201.

[64] H. Dorn, K. Egner, Brandversuche Mit Geleimten Holzbauteilen, 1961.

[65] J.R. Martins, A. Ning, Engineering Design Optimization, Cambridge University Press, 2021.

[66] A. Der Kiureghian, J.-B. Ke, The stochastic finite element method in structural reliability, Probab. Eng. Mech. 3 (2) (1988) 83–91.

[67] M.H. Faber, S. Rostam, Durability and service life of concrete structures—The owners' perspective, in: Proc., Int. Conf. on Safety, Risk and Reliability, IABSE, Zurich, 2021, pp. 369–374.

[68] E.H. Vanmarcke, Random Field: Analysis and Synthesis, Press, Cambridge, Mass., 1983.

[69] K.A. Vu, M.G. Stewart, Predicting the likelihood and extent of reinforced concrete corrosion-induced cracking, J. Struct. Eng. 131 (11) (2005) 1681–1689.

[70] EN-338, Structural timber — Strength class, 2009, Uni.

[71] J.J. Remmers, R. de Borst, A. Needleman, The simulation of dynamic crack propagation using the cohesive segments method, J. Mech. Phys. Solids 56 (1) (2008) 70–92, http://dx.doi.org/10.1016/j.jmps.2007.08.003, URL https://www.sciencedirect.com/science/article/pii/S0022509607001706. Bridging scales in mechanics - "Where are the bottom and the top?" The Needleman-Tvergaard Solid Mechanics Symposium.

[72] J.-H. Song, P.M.A. Areias, T. Belytschko, A method for dynamic crack and shear band propagation with phantom nodes, Internat. J. Numer. Methods Engrg. 67 (6) (2006) 868–893, http://dx.doi.org/10.1002/nme.1652, arXiv:https://onlinelibrary.wiley.com/doi/pdf/10.1002/nme.1652. URL https://onlinelibrary.wiley.com/doi/abs/10.1002/nme.1652.

[73] E.S. Flores, K. Saavedra, J. Hinojosa, Y. Chandra, R. Das, Multi-scale modelling of rolling shear failure in cross-laminated timber structures by homogenisation and cohesive zone models, Int. J. Solids Struct. 81 (2016) 219–232, http://dx.doi.org/10.1016/j.ijsolstr.2015.11.027, URL https://www.sciencedirect.com/science/article/pii/S0020768315004898.

[74] D. Rammer, L. Soltis, Experimental Shear Strength of Glulam-Laminated Beams, Research Paper: FPL-RP 527, Forest Products Laboratory, 1994, pp. 1–38.

[75] D.R. Rammer, Experimental Shear Strength of Unchecked Solid-Sawn Douglas-Fir, Vol. 553, US Department of Agriculture, Forest Service, Forest Products Laboratory, 1996.

[76] J. Longworth, Longitudinal shear strength of timber beams, Forest Prod. J. 27 (8) (1997) 19–23.

[77] B.J. Yeh, Shear Strength of Douglas-Fir Structural Glued-Laminated Timber, American Wood Systems-American Plywood association, 1993.